

Basic Properties and Design Principles of UWB Antennas

Selection of suitable antennas from the many existing types, based on understanding their characteristics, is essential for effective ultrawide-band system design.

By WERNER WIESBECK, *Fellow IEEE*, GRZEGORZ ADAMIUK, *Student Member IEEE*, AND CHRISTIAN STURM, *Student Member IEEE*

ABSTRACT | Basic principles for ultra-wide-band (UWB) radiation are presented and discussed in this paper. The discussion starts with a description of the influence of antennas on UWB transmission. The parameters characterizing antennas in time and in frequency domain are specified. Since the number of possible antenna structures is nearly unlimited, the focus will be on a classification according to different radiation principles. For each of these mechanisms, the typical advantages and disadvantages are discussed, and an example antenna and its characteristics are presented. For a wireless engineer, the problem to solve is the proper design of an antenna with the desired radiation characteristics. The final outcome of this paper is that there exist numbers of UWB antennas, but not each of them is suited for any application, especially in view of radar and communication systems requirements.

KEYWORDS | Ultra-wide-band (UWB); UWB antenna characterization; UWB link; UWB transfer functions

I. UWB SIGNAL TRANSFER CHARACTERIZATION

Typically, narrow-band antennas and propagation are described in the frequency domain. Usually the characteristic parameters are assumed to be constant over a few percent bandwidth. For ultra-wide-band (UWB) systems, the frequency-dependent characteristics of the antennas and the frequency-dependent behavior of the channel have

to be considered. On the other hand, UWB systems are often realized in an impulse-based technology, and therefore the time-domain effects and properties have to be known as well [1]. Hence there is a demand for both a frequency-domain representation and a time-domain representation of the system description. In the following, these characterizations in the frequency domain and in the time domain are presented. All parameters are uniformly used in the whole paper but may not be necessarily compliant with the denotation presented in the cited literature. The coordinate system throughout this paper is as shown in Fig. 1.

A. UWB Frequency-Domain Signal Link Characterization

For the frequency-domain description, it is assumed that the transmit antenna is excited with a continuous-wave signal with the frequency f . The relevant parameters for the frequency-domain link description are:

- amplitude of transmit signal $U_{Tx}(f)$ in [V];
- amplitude of receive signal $U_{Rx}(f)$ in [V];
- radiated field strength at position \mathbf{r} $\mathbf{E}_{Tx}(f, \mathbf{r}, \theta_{Tx}, \psi_{Tx})$ in [V/m];
- transfer function of the transmit antenna $\mathbf{H}_{Tx}(f, \theta_{Tx}, \psi_{Tx})$ in [m];
- transfer function of the receive antenna $\mathbf{H}_{Rx}(f, \theta_{Rx}, \psi_{Rx})$ in [m];
- characteristic transmit antenna impedance $Z_{C,Tx}(f)$ in [Ω];
- characteristic receive antenna impedance $Z_{C,Rx}(f)$ in [Ω];
- antenna gain $G(f, \theta, \psi)$;
- distance between Tx-Rx antennas r_{TxRx} in [m].

The antenna transfer functions represent a two-dimensional vector with two orthogonal polarization

Manuscript received September 13, 2007; revised March 26, 2008. Current version published March 18, 2009.
The authors are with the Institut für Hochfrequenztechnik und Elektronik, Universität Karlsruhe (TH), 76131 Germany (e-mail: werner.wiesbeck@kit.edu).

Digital Object Identifier: 10.1109/JPROC.2008.2008838

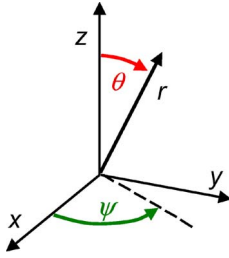


Fig. 1. Coordinate system for UWB link and antenna characterization.

components H_{C_0} and H_X . The dimension of the transfer functions is meter, and they are equivalent to effective antenna heights, dependent on frequency [2]. The characteristic antenna impedances define the air interface reflection coefficients. $\mathbf{H}_{T_x}(f, \theta_{T_x}, \psi_{T_x})$ is the transfer function that relates the transmit signal $U_{T_x}(f)$ to the radiated field strength $\mathbf{E}_{T_x}(f, \mathbf{r})$ for an antenna in the transmit mode [see (1)]

$$\frac{\mathbf{E}_{T_x}(f, \mathbf{r})}{\sqrt{Z_0}} = \frac{e^{j\omega r_{T_x R_x}/c_0}}{2\pi r_{T_x R_x} c_0} \mathbf{H}_{T_x}(f, \theta_{T_x}, \psi_{T_x}) \cdot j\omega \frac{U_{T_x}(f)}{\sqrt{Z_{C,T_x}}}. \quad (1)$$

$\mathbf{H}_{R_x}(f, \theta_{R_x}, \psi_{R_x})$ is the transfer function that relates the received signal amplitude $U_{R_x}(f)$ to the incident field $\mathbf{E}_{R_x}(f, \mathbf{r})$ (in the frequency domain) for an antenna in the receive mode [see (2)]. The transfer functions are reciprocal, $\mathbf{H}_{T_x} = \mathbf{H}_{R_x}$, but the direction of the signal flow with respect to the coordinate system has to be taken into account. With these parameters, the Tx-Rx link is given in Fig. 2, including the channel. The small graphs symbolize the typical influence of the link contributions. The initial chirp and its derivative are sketched.

In the frequency-domain description, the consecutive subsystem parameters are multiplied. The total analytical

description of a free space UWB propagation link is given by (2)

$$\frac{U_{R_x}(f)}{\sqrt{Z_{C,R_x}}} = \mathbf{H}_{R_x}^T(f, \theta_{R_x}, \psi_{R_x}) \cdot \frac{e^{j\omega r_{T_x R_x}/c_0}}{2\pi r_{T_x R_x} c_0} \cdot \mathbf{H}_{T_x}(f, \theta_{T_x}, \psi_{T_x}) \cdot j\omega \frac{U_{T_x}(f)}{\sqrt{Z_{C,T_x}}}. \quad (2)$$

Two orthogonal polarizations are included in the Tx and Rx transfer functions, as noted above. While in narrow-band systems the radiation angles θ and ψ influence only the polarization, amplitude, and the phase of the signal, they influence additionally the entire frequency-dependent signal characteristics in UWB systems.

For UWB links in rich scattering environments, e.g., indoor, the influence of the channel can be described by a frequency-dependent polarimetric channel transfer matrix [3].

B. Time-Domain Signal Link Characterization

For the time-domain description, it is assumed that the transmit antenna is excited with a impulse. The elements of the UWB time domain link characterization are:

- amplitude of transmit signal $u_{T_x}(t)$ in [V];
- amplitude of receive signal $u_{R_x}(t)$ in [V];
- impulse response of the transmit antenna $\mathbf{h}_{T_x}(t, \theta_{T_x}, \psi_{T_x})$ in [m/ns];
- impulse response of the receive antenna $\mathbf{h}_{R_x}(t, \theta_{R_x}, \psi_{R_x})$ in [m/ns];
- radiated field strength $\mathbf{e}_{T_x}(t, \mathbf{r}, \theta_{T_x}, \psi_{T_x})$;
- distance between Tx-Rx antennas $r_{T_x R_x}$ in [m].

In the time domain, the antenna's transient response $\mathbf{h}(t, \theta, \psi)$ becomes more adequate for the description of impulse systems. The antenna's transient response is dependent on time, but also on the angles of departure θ_{T_x}, ψ_{T_x} , respectively, angles of arrival θ_{R_x}, ψ_{R_x} , and polarization [4]. As a consequence, the antennas do not radiate the same pulse in all directions. This may cause severe problems in communications and radar as well. It is

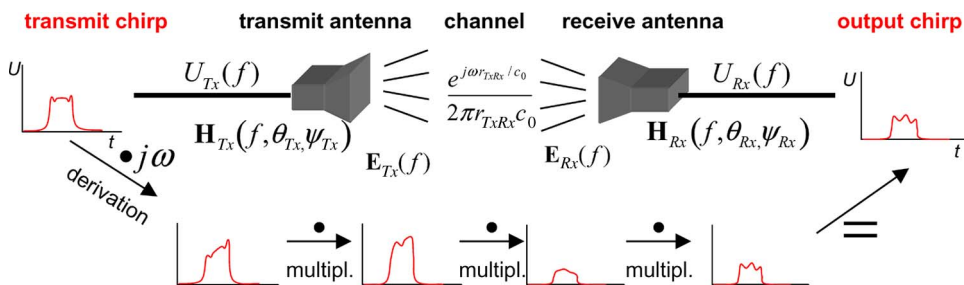


Fig. 2. Frequency-domain system link level characterization.

very important to include in system descriptions the angular behavior of the antennas since all transmitted or received paths, e.g., in indoor applications, are weighted by the antenna patterns and therefore contribute with different time domain characteristics, e.g., polarization, amplitude, phase, and delay to the received voltage $u_{Rx}(t)$. In Fig. 3, the time-domain link level scheme is shown. The small graphs symbolize the typical influence of the link contributions. The initial pulse and its derivative are sketched.

Any antenna differentiates any signal, because antennas do not radiate dc signals. Equations (1) and (2) have, after conversion to the time domain, the form presented in (3) and (4), respectively. Fundamental operations like the multiplication in the frequency domain are substituted by convolution in the time domain. Equation (3) relates the radiated field strength $e_{Tx}(t, \mathbf{r})$ to the excitation voltage $u_{Tx}(t)$ and the transient response of the transmit antenna $\mathbf{h}_{Tx}(t, \theta_{Tx}, \psi_{Tx})$ [5]. In (4), again only free-space propagation is regarded (line of sight Tx-Rx)

$$\frac{e_{Tx}(t, \mathbf{r})}{\sqrt{Z_0}} = \frac{1}{2\pi r_{TxRx} c_0} \delta\left(t - \frac{r_{TxRx}}{c_0}\right) * \mathbf{h}_{Tx}(t, \theta_{Tx}, \psi_{Tx}) * \frac{\partial u_{Tx}(t)}{\partial t \sqrt{Z_{C,Tx}}} \quad (3)$$

$$\frac{u_{Rx}(t)}{\sqrt{Z_{C,Rx}}} = \mathbf{h}_{Rx}^T(t, \theta_{Rx}, \psi_{Rx}) * \frac{1}{2\pi r_{TxRx} c_0} \delta\left(t - \frac{r_{TxRx}}{c_0}\right) * \mathbf{h}_{Tx}(t, \theta_{Tx}, \psi_{Tx}) * \frac{\partial u_{Tx}(t)}{\partial t \sqrt{Z_{C,Tx}}} \quad (4)$$

The delay time of the channel is taken care of by the antenna spacing r_{TxRx} . The transient response functions are also reciprocal, $\mathbf{h}_{Tx} = \mathbf{h}_{Rx}$, but the direction of signal flow with respect to the coordinate system has to be taken into account.

The antennas are an essential part of any wireless system, and their properties have to be carefully taken into account during all steps of the system design. For UWB impulse systems, this is vital.

II. UWB DEFINITIONS AND ANTENNA PARAMETERS

The desired operating frequencies are given by:

- U.S. FCC regulation [6] as 3.1 to 10.6 GHz;
- European regulation [7] (2007|131|EC) as 6.0 to 8.5 GHz;
- special allocations, e.g., ground penetrating radar or wall radar;

but not limited to these. A general definition of UWB is stated with the relative bandwidth

$$2(f_H - f_L)/(f_H + f_L) > 0.2 \quad (5)$$

where f_H and f_L are the upper and lower band limits, respectively. Relative bandwidths in excess of 100% are possible for some antenna types.

A. Antenna Characterization Parameters

In contrast to classic narrow-band antenna theory, where the antenna characteristics are regarded for only a small bandwidth, the characterization of antennas over an ultrawide frequency range requires new specific quantities and representations [1], [8]. In this section, both time-domain and frequency-domain representations are regarded. Depending on the application, the relevant ones have to be selected. In general, the Fourier transforms forward and backward are the operations to switch from frequency domain to time domain, and vice versa.

An impulse fed to an UWB antenna is subject to:

- differentiation;
- dispersion (energy storage);
- radiation;
- losses (dielectric/ohmic).

The antenna's complete behavior, including frequency dependency, can be described by the linear system theory. The characteristics are expressed either by a time-domain impulse response $\mathbf{h}(t, \theta_{Tx}, \psi_{Tx})$ or by the frequency-domain transfer function $\mathbf{H}(f, \theta_{Tx}, \psi_{Tx})$, as given earlier, both of which contain the full information on the antenna radiation. The dispersion of the antenna can be analyzed by regarding the analytic impulse response, which is

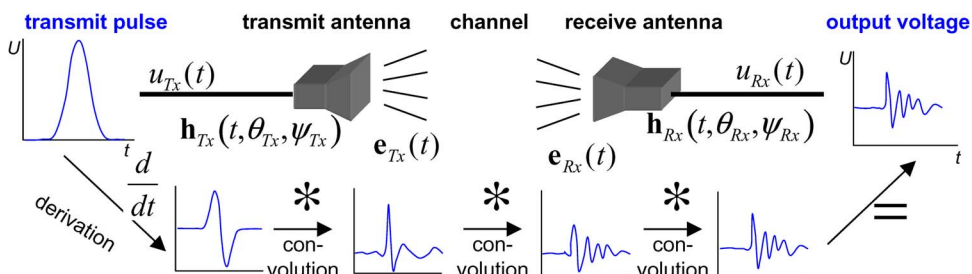


Fig. 3. UWB system link level characterization in time domain.

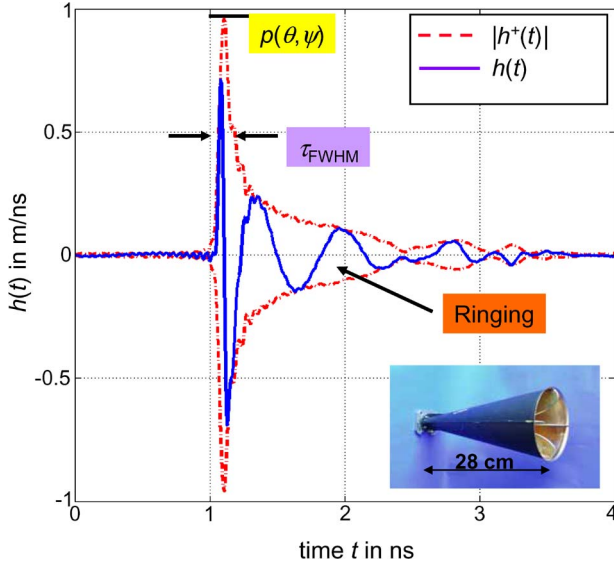


Fig. 4. Characterization of the antenna time-domain transient response (here: horn antenna).

calculated by the Hilbert transform \mathcal{H} commonly used in signal processing.

$$h^+(t) = (h(t) + j\mathcal{H}\{h(t)\}). \quad (6)$$

The envelope $|h^+(t)|$ of the analytic impulse response localizes the distribution of energy versus time and is hence a direct measure for the dispersion of an antenna.

Typical examples of measured antenna impulse responses $h(t)$ and $|h^+(t)|$ are shown in Fig. 4 for a given polarization and direction (θ, ψ) of radiation with the further characteristic parameters for the peak pulse value $p(\theta, \psi)$, the width of the pulse full-width at half-maximum (FWHM), and the ringing duration τ_r . Note that all parameters are dependent on polarization and spatial coordinates $r(\theta, \psi)$.

Examples for specific quantities are given later for the presented antennas.

1) *Peak Value of the Envelope*: The peak value $p(\theta, \psi)$ of the analytic envelope $|h^+(t)|$ is a measure for the maximal value of the strongest peak of the antenna's time-domain transient response envelope. It is mathematically defined as

$$p(\theta, \psi) = \max_t |h^+(t, \theta, \psi)| \text{ in } \frac{\text{m}}{\text{ns}}. \quad (7)$$

A high peak value $p(\theta, \psi)$ is desirable.

2) *Envelope Width*: The envelope width describes the broadening of the radiated impulse and is defined as the

width of the magnitude of the analytic envelope $|h^+(t)|$ at half maximum (FWHM). Analytically, it is defined as

$$\tau_{\text{FWHM}} = t_1|_{|h^+(t_1)|=p/2} - t_2|_{|h^+(t_2)|=p/2} \text{ in ns.} \quad (8)$$

The envelope width should not exceed a few hundred picoseconds in order to ensure high data rates in communications or high resolution in radar applications.

3) *Ringing*: The ringing τ_r of a UWB antenna is undesired and usually caused by resonances due to energy storage or multiple reflections in the antenna. It results in oscillations of the radiated pulse after the main peak. The duration of the ringing τ_r , which is defined as the time until the envelope has fallen from the peak value $p(\theta, \psi)$ below a certain lower bound $\alpha \cdot p(\theta, \psi)$, is measured as follows:

$$\tau_{r=\alpha} = t_1|_{h^+(t_1)=\alpha p} - t_2|_{t_2 < t_1 \wedge h^+(t_2)=p} \text{ in ns.} \quad (9)$$

The duration τ_r of the ringing of a UWB antenna should be negligibly small, i.e., less than a few envelope widths τ_{FWHM} . The energy contained in ringing is of no use at all; it lowers the peak value $p(\theta, \psi)$. It can therefore be eliminated by, e.g., absorbing materials.

4) *Transient Gain*: The transient gain $g_T(\theta, \psi)$ is an integral quality measure that characterizes the ability of an antenna to radiate the power of a given waveform $u_{\text{Tx}}(t)$

$$\begin{aligned} g_T(\theta, \psi) &= \frac{\left\| h(t, \theta, \psi) * \frac{du_{\text{Tx}}(t)}{dt} \right\|^2}{\left\| \sqrt{\pi c_0} u_{\text{Tx}}(t) \right\|^2} \\ &= \frac{\left\| H(\omega, \theta, \psi) j\omega U_{\text{Tx}}(f) \right\|^2}{\left\| \sqrt{\pi c_0} U_{\text{Tx}}(f) \right\|^2} \end{aligned} \quad (10)$$

where the norm is defined by

$$\|f(x)\| = \int_{-\infty}^{\infty} |f(x)| dx. \quad (11)$$

5) *Gain in Frequency Domain*: The gain in frequency domain is defined like in narrow-band systems. It can be calculated from the antenna transfer function

$$G(f, \theta, \psi) = \frac{4\pi f^2}{c_0^2} |H(f, \theta, \psi)|^2. \quad (12)$$

It is important that the transfer function is multiplied by f^2 .

6) *Group Delay*: The group delay $\tau_g(\omega)$ of an antenna characterizes the frequency dependence of the time delay. It is defined in frequency domain

$$\tau_g(\omega) = -\frac{d\varphi(\omega)}{d\omega} = -\frac{d\varphi(f)}{2\pi df} \quad (13)$$

where $\varphi(f)$ is the frequency-dependent phase of the radiated signal.

Of interest is also the mean group delay $\bar{\tau}_g$, as it is a single number for the whole UWB frequency range

$$\bar{\tau}_g = \frac{1}{\omega_2 - \omega_1} \int_{\omega_1}^{\omega_2} \tau_g(\omega) d\omega. \quad (14)$$

A nondistorted structure is characterized by a constant group delay, i.e., linear phase, in a relevant frequency range. The nonlinearities of a group delay indicate the resonant character of the device, which implicates the ability of the structure to store the energy. It results in ringing and oscillations of the antenna impulse response $h(t)$ [9]. A measure for the constancy of the group delay is the deviation from the mean group delay $\bar{\tau}_g$, denoted as relative group delay $\tau_{g,\text{rel}}(\omega)$ (15)

$$\tau_{g,\text{rel}}(\omega) = \tau_g(\omega) - \bar{\tau}_g. \quad (15)$$

Examples of the relative group delay of the Vivaldi antenna and the logarithmic periodic dipole array (Log-Per) antenna (see Section III-A and D) in the frequency range from 3 to 11 GHz are shown in Fig. 5. In the case of the Vivaldi antenna, which is a nonresonant structure, the relative group delay shows only weak and slow oscillations over the whole frequency band. On the other side, the relative group delay of the Log-Per antenna shows strong and sharp oscillations over the whole frequency band, which results in an oscillation of the antenna impulse response $h_{\text{Log-Per}}(t)$. For this antenna, the group delay is frequency dependent, and lower frequencies show a higher relative group delay. It is caused by the frequency-dependent phase centers of the radiation.

III. UWB ANTENNA PRINCIPLES

The radiation of guided waves has been discussed intensively in the past. It is the common understanding that the key mechanism for radiation is *charge acceleration* [10], [11]. The question to answer for UWB is: what kind of

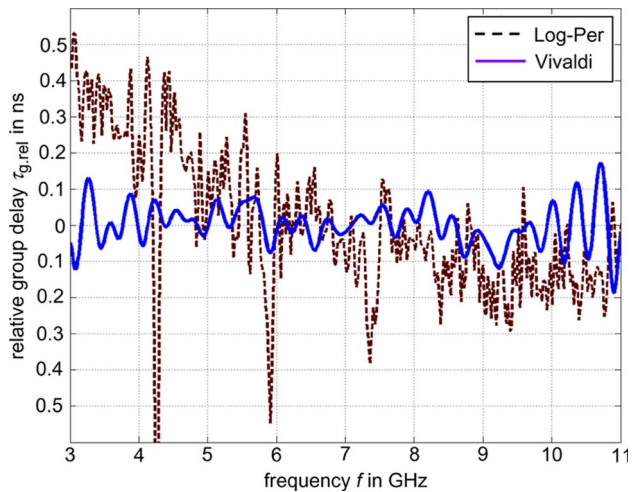


Fig. 5. Relative group delay $\tau_{g,\text{rel}}(f)$ of a Vivaldi antenna and a Log-Per antenna.

structures facilitates the charge acceleration over a very wide bandwidth? The ultrawide bandwidth radiation is based on a few principles:

- traveling-wave structures;
- frequency-independent antennas (angular constant structures);
- self-complementary antennas;
- multiple resonance antennas;
- electrically small antennas.

In most cases the radiation starts where the electric field connects 180° out-of-phase currents with half a wavelength spacing. Many antennas radiate by a combination of two or more of the above principles and can therefore not be simply classified.

In the following, the relationships between the radiation principles and the properties of the antennas are discussed. Each explanation of the radiation phenomenon is supported by an example of an antenna.

A. Traveling-Wave Antennas

Traveling-wave antennas offer for the guided wave a smooth, almost not recognizable transition with the fields accelerated to free-space propagation speed c_0 . Typical antennas are tapered wave guide antennas [12]—for example, the horn antenna (see Fig. 4) or the Vivaldi antenna (see Fig. 6). Other radiating traveling-wave structures are, e.g., the slotted waveguide or the dielectric rod antenna. Here the focus will be on the Vivaldi antenna as an example, for which different feed structures like microstrip line, slot line, and antipodal can be applied.

The Vivaldi antenna guides the wave from the feed in a slot line to a wide-band taper. The exponential taper is a priori wide-band, because it offers for all frequencies within the given bandwidth the proper radiation condition. Other tapers, like polynomial tapers or any other



Fig. 6. Aperture coupled Vivaldi antenna. (Left) Top view; (right) bottom view with feed line. Substrate size $75 \times 78 \text{ mm}^2$.

mathematical function that provides a smooth transition, can be used and optimized, regarding the input reflection coefficient and the radiation characteristics. A typical structure is shown in Fig. 6, etched on a dielectric substrate. The Vivaldi is fed at the narrow side of the slot. For UWB, the major tasks are the wide-band frequency-independent feed and slot-line terminations. The feed shown here is designed with a Marchand balun network with aperture coupling. Nonresonant aperture coupling is usually a good choice for UWB feed structures. This allows also for an impedance matching in a wide range. A stub, and the slot line by a circular shaped cavity, terminate the microstrip feed line. The antenna can be designed relatively compact. The propagation velocity v on the structure changes from the slot-line wave velocity v_{sl} to c_0 at the end of the taper. It varies only slightly with frequency. The Vivaldi antenna's time-domain transient response in the E -plane is shown in Fig. 7. This, for narrow-band antennas' unusual representation, displays the impulse distortion by the antenna in time t versus the E -plane angle ψ . The Vivaldi antenna has a rather low

distortion compared to other UWB antennas. The high peak value ($p = 0.35 \text{ m/ns}$) and the short duration of the transient response envelope [$(\tau_{FWHM} = 135 \text{ ps})$; see Fig. 4] stand for very low dispersion and ringing. The ringing of the antenna is due to multiple reflections at the substrate edges and parasitic currents along the outer substrate edges. The ringing can be reduced by enlarging the transverse dimensions of the antenna, by metal flares or by chokes. Absorbing materials around the substrate edges reduce the ringing without influencing the other characteristics of the transient response. The slightly asymmetric impulse response results from the feed line. The frequency- and angle-dependent gain $G(f, \theta = 90^\circ, \psi)$ in Fig. 8 is calculated from the measured directional transfer function $H(f, \theta = 90^\circ, \psi)$. The gain is quite constant versus frequency in the main beam direction. The maximum gain G_{\max} is 7.9 dBi at 5.0 GHz; at the lower frequencies, close to 3 GHz, small resonances are visible. The average gain \bar{G} in the FCC frequency band is 5.7 dBi. The main parameters of the Vivaldi antenna are summarized in Table 1.

The Vivaldi antenna is well suited for direct planar integration and also for UWB antenna arrays for radar and communications. In the past it has been used for special cases of high power radiation.

B. Frequency-Independent Antennas

Rumsey investigated the fundamentals of frequency-independent antennas in the 1960s [13]. He observed that a scaled version of a radiating structure must exhibit the same characteristics like the original one, when fed with a signal whose wavelength is scaled by the same factor. As a consequence, if the shape of an antenna is invariant to physical scaling, its radiating behavior is expected to be independent of frequency. The typical realization is an angular constant structure, which is described only by

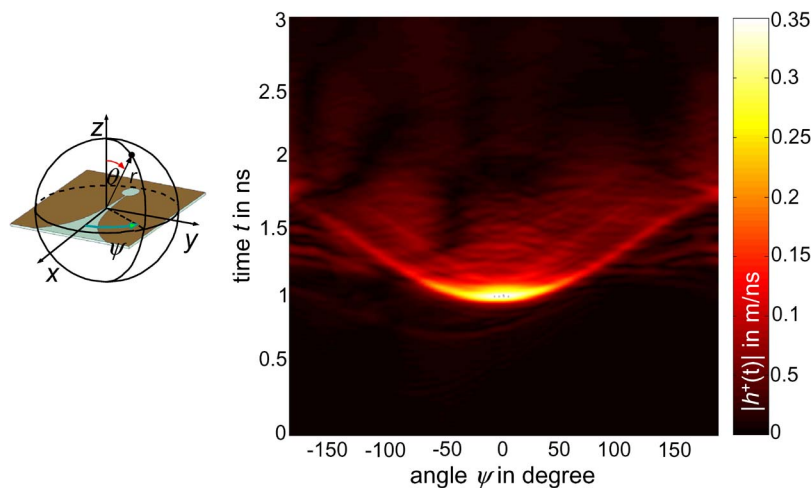


Fig. 7. Measured impulse response $|h^+(t, \theta)|$ of the Vivaldi antenna of Fig. 6 in E -plane versus frequency.

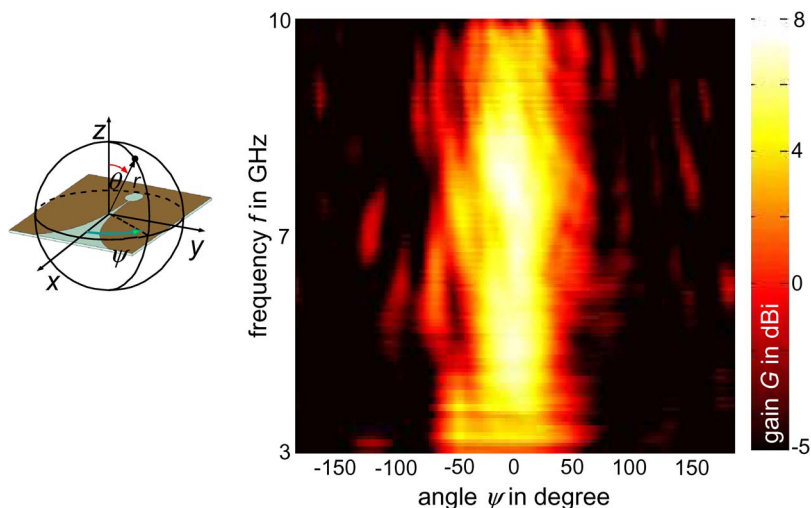


Fig. 8. Measured gain $G(f, \theta = 90^\circ, \psi)$ of the Vivaldi antenna of Fig. 6 in E-plane versus frequency.

angles. It must be noted that the independence from frequency does not necessarily refer to the input impedance of the structure. In order to obtain a constant input impedance, additional principles like those described in Section III-C have to be applied.

The scaling usually involves constant angles. It is possible to define a “truncation principle” to apply this concept to the practical case, where the size of any physical object is obviously finite [14]. In fact, provided that the overall current on the antenna tends to decrease due to the radiation, when moving away from the feeding point, it is possible to define a limited “active” region, where the current falls below relevant values. If the actual, finite antenna contains this area, it can be assumed that the truncation of the geometry does not modify the behavior of the antenna around the chosen wavelength. A typical example of a frequency-independent antenna is the biconical antenna [15].

A planar example of the biconical antenna is the bowtie antenna. The antenna structure consists of two triangular metal sheets (see Fig. 9). They are usually fed by a symmetric line (twin line), which is matched to the feed

point impedance. In the case of an asymmetric feed line (like coaxial or microstrip lines), a balun transformer is needed. The bowtie antenna has for the FCC UWB frequency band reasonable dimensions. The application of aperture feed and further optimizations allow very compact design.

The aperture coupled bowtie antenna consists of two triangular radiating patches, of which one serves as a ground plane for the tapered microstrip feed line that ends with a broadband stub (see Fig. 9). The feeding structure couples the energy from an asymmetric microstrip line to the radiating bowtie elements through the aperture formed

Table 1 UWB Parameters of the Vivaldi Antenna of Fig. 6 in Main Beam Direction

Parameter	Value
p_{\max} in m/ns	0.35
τ_{FWHM} in ps	135
\bar{G} in dBi	5.7
G_{\max} in dBi	7.8
$\tau_{r=0,22}$ in ps	150

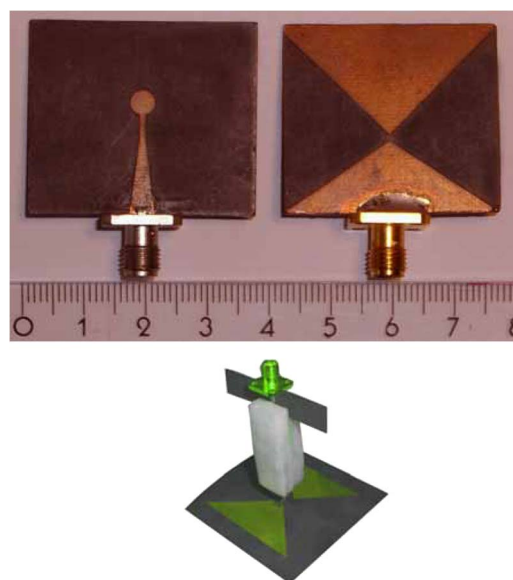


Fig. 9. (Left) Aperture coupled bowtie antenna; bottom view with feed line. (Right) Top view; symmetric fed bowtie antenna with balun.

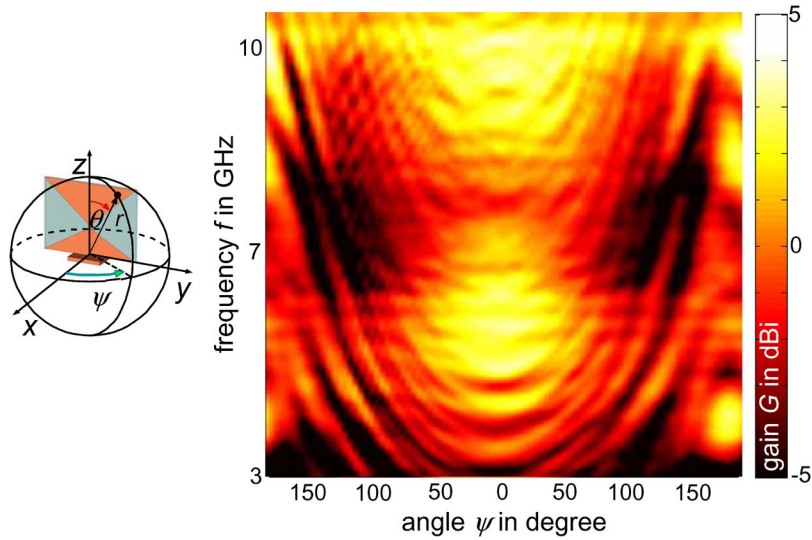


Fig. 10. Measured gain $G(f, \theta = 90^\circ, \psi)$ of an aperture coupled bowtie antenna in H-plane versus frequency.

by the tips of the triangles. Therefore the antenna is called aperture coupled bowtie antenna. This feeding technique is basically similar to the operation of the well-known microstrip slot-line transitions with a Marchand balun. Almost no additional ringing is introduced by this coupling mechanism. The pulses on the radiating elements are traveling faster than those on the line, due to the lower effective $\epsilon_{r,eff}$. This is compensated by the fact that the stub length is shorter than the length of the radiating elements.

The aperture-coupled bowtie antenna has a nearly omnidirectional radiation pattern in the H-plane (Fig. 10). Therefore this type of antenna can find application, e.g., in communications in mobile devices. It can be realized quite

small. Fig. 11 presents the measured impulse response $|h^+(t)|$ of the antenna in Fig. 9. The almost omnidirectional radiation in H-plane is well visible, accompanied by a small ringing of the antenna.

Other types of antennas with frequency-independent characteristics might be some versions of logarithmic-periodic antennas or spiral antennas [16]. Although these antennas can show frequency-independent characteristics, they are based on a different design principle, and their properties are different compared to those described above. In general, antennas may combine more than one radiation principle and may change the radiation principle versus frequency.

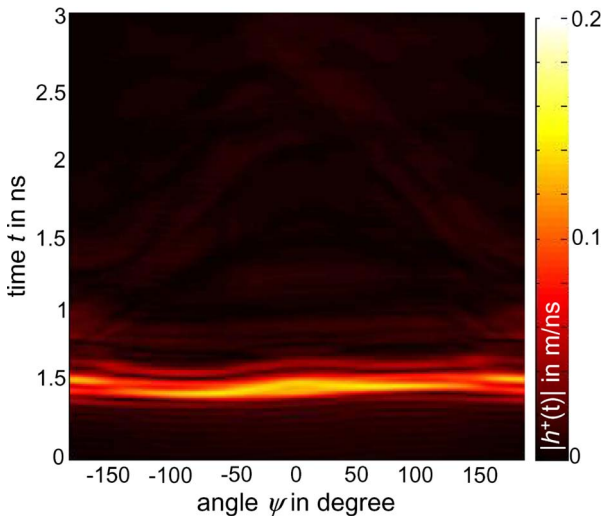


Fig. 11. Measured impulse response $|h^+(t)|$ of the bowtie antenna in H-plane.

C. Self-Complementary Antennas

Self-complementary antennas are characterized by a self-complementary metallization [17]. This means that metal can be replaced by dielectric and vice versa without

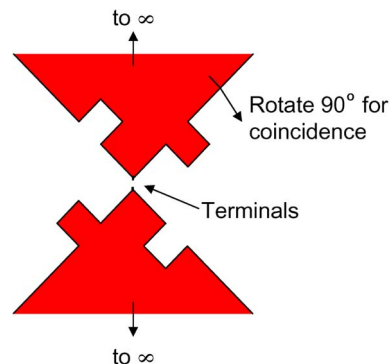


Fig. 12. Truncated fractal antenna to show the principle of self-complementary antennas.



Fig. 13. Self-complementary antennas. (Left) Two-arm logarithmic spiral antenna and (right) sinuous antenna.

changing the antenna’s structure (Fig. 12). The behavior of self-complementary structures can be analyzed by applying Babinet’s principle [18]. This results in an invariant input impedance of

$$Z_{in} = Z_{F0}/2 = 60\pi\Omega \tag{16}$$

with Z_{F0} being the free-space impedance. Self-complementary structures only guarantee a constant input impedance, but not necessarily constant radiation characteristics independent from frequency. It is also possible to design structures that are similar to self-complementary structures but have an unbalanced ratio of metalized to nonmetalized areas. These structures exhibit an input impedance that is nearly constant versus frequency but different from $Z_{F0}/2$ [19]. For exact description of self-complementary antennas, the reader is referred to [20]. Typical candidates are the 90° bowtie antenna, the sinuous antenna, the logarithmic spiral antenna [21], or some fractal antennas [22].

An example of a two-arm logarithmic spiral antenna is shown in Fig. 13. This antenna realizes the principle of frequency independence; the metallization is only defined by angles, and it follows Babinet’s principle. The two arms

of the antenna are fed in the center with a symmetric line with an impedance of $Z_L = 60\pi\Omega$. When properly designed, the logarithmic spiral antenna radiates where the two arms are spaced by $\lambda/2$, i.e., where the circumference is $\lambda\pi/2$. By a proper dimensioning of the structure, the antenna can be made broadband up to several 100% bandwidth.

The principle of radiation can be seen by plotting the current distribution into the antenna of Fig. 14. The diameter of the outer arms reaches 40 cm in this case. In Fig. 14(a), the antenna is excited with the frequency of 300 MHz and in (b) with 450 MHz. It can be noted that at lower frequencies, where the wavelength is longer, the high current amplitudes occur at a larger diameter on the spiral than in the case of the higher frequency of 450 MHz. The “vanishing” of the currents outside of the maximum currents indicates that energy has been radiated.

The logarithmic spiral antenna is a directional antenna with two main beams orthogonal to the spiral plane. The radiated wave is circularly polarized, provided the pulse length covers 360° of the radiating circumference. The polarizations in the two main radiation directions are orthogonal to each other. One beam is usually suppressed by absorbing material. It prevents propagation of the orthogonal polarization simultaneously.

The frequency dependence of the position of the radiating area and therefore frequency-dependent time delays result in a broadening and a smaller peak value of the antenna impulse response, compared to, e.g., the Vivaldi antenna.

As another candidate for the visualization of the characteristics of frequency-independent antennas, the Archimedian spiral antenna is analyzed. This antenna has, compared to the logarithmic spiral antenna, constant line width and spacing, and these are usually identical. Due to the close separation of adjacent lines, they couple strongly. This causes the radiation where adjacent lines are in phase, i.e., where the circumference is λ . To analyze the transmitted pulse characteristic, in the simulation tool a

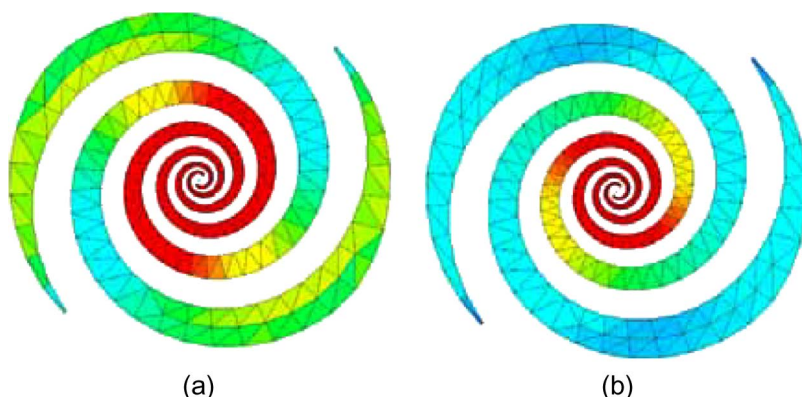


Fig. 14. Current distribution on a logarithmic spiral antenna: (a) $f = 300$ MHz and (b) $f = 450$ MHz.

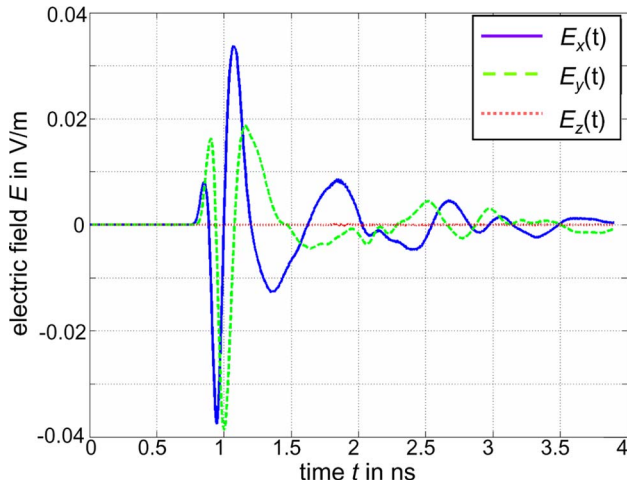


Fig. 15. Simulation of the received electric field $e_{rx}(t)$ from an Archimedean spiral antenna (xy-plane) with linear polarized electric field probes in x-, y-, z-direction; input pulse is a Gauss pulse with $\tau_{FWHM} = 88$ ps.

linearly polarized electric field probe is set in the far field of the Archimedean spiral antenna. The electric field probes are arranged along the x-, y-, and z-axis, whereas the antenna is positioned in the xy-plane. The received electric field $e_{rx}(t)$ of a simulation of this configuration excited with a $\tau_{FWHM} = 88$ ps Gauss pulse is shown in Fig. 15. The radiated UWB signal has a strong, short peak with a reasonable ringing. Since the radiated pulse is circularly polarized, both $e_x(t)$ and $e_y(t)$ components are present. The $e_z(t)$ components are not excited since the radiated wave is a transverse electromagnetic mode wave. A problem of all spiral antennas for UWB operation may be the rotation of the radiated field vector with frequency. It has to be kept in mind that for a pulsed mode operation, the pulse duration has to be sufficient in order to cover 360° of field vector orientation for circular polarization.

D. Multiple Resonance Antennas

Multiple resonance antennas are combinations of multiple, narrow-band, radiating elements. Each element—for example, a dipole—covers a limited bandwidth, e.g., 20% of the total UWB bandwidth. Typical candidates are the Log-Per [23] and fractal antennas.

The planar Log-Per antenna (Fig. 16) consists of n adjoining unit cells (dipoles), with the dimensions l_μ of adjacent cells scaled by $\log(l_\mu/l_{\mu+1}) = \text{constant}$ [24]. Each dipole is etched with one half on the top layer and the other half on the bottom layer of the substrate. The antenna is fed, for example, by a coaxial line via a triplate line inside the structure at the high-frequency port. This structure can be optimized for low return loss ($S_{11} < -10$ dB) in the whole FCC UWB frequency band. The design of the antenna is compact ($60 \times 50 \times 2$ mm³), with 3 dB beamwidths $\psi_{3\text{dB}} \approx 65^\circ$ in the E-plane and

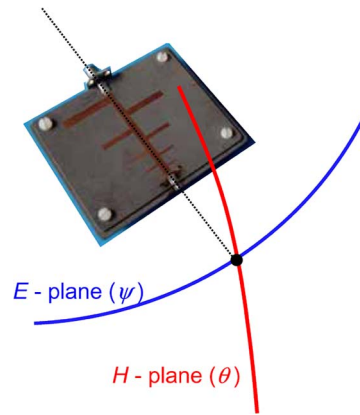


Fig. 16. Log-Per antenna with a coaxial connector feeding the inner triplate line.

H in the H-plane. These values are quite constant over the desired frequency range. As can be seen from Fig. 17, the impulse response of the Log-Per antenna exhibits strong oscillations. This can be explained by the consecutively excited ringing of coupled, resonating dipoles.

For reasons of comparison with other antennas, Fig. 17 shows the transient response $h(t, \psi)$, $\theta = 0$ versus the E-plane angle ψ and time t . The broadening of the impulse response compared to the Vivaldi antenna is obvious. Consequently, the peak value p of the antenna impulse response reduces to only 0.13 m/ns. It is due to the resonant structure of the radiating dipoles. Any UWB antenna with resonant elements broadens the radiated impulse, i.e., increases the τ_{FWHM} and lowers the peak value p .

Fig. 18 is a cut in the main beam of the transient response $h(t, \psi)$, $\theta = 0$. The resonant character of the Log-Per antenna is even more obvious in this representation,

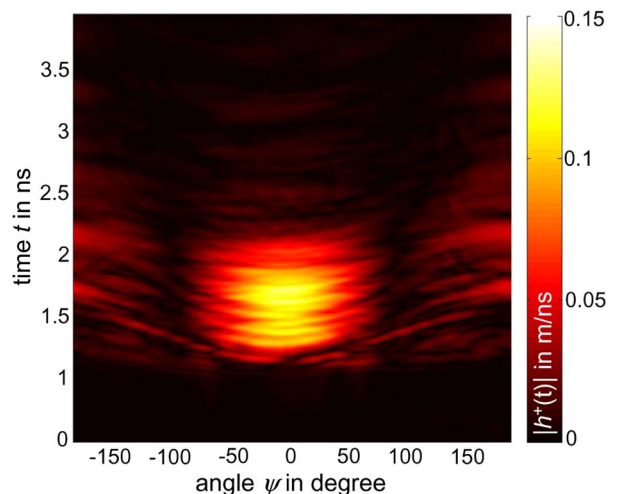


Fig. 17. Measured impulse response $|h^+(t, \psi)|$, $\theta = 0$ of the Log-Per antenna (Fig. 16) in the E-plane.

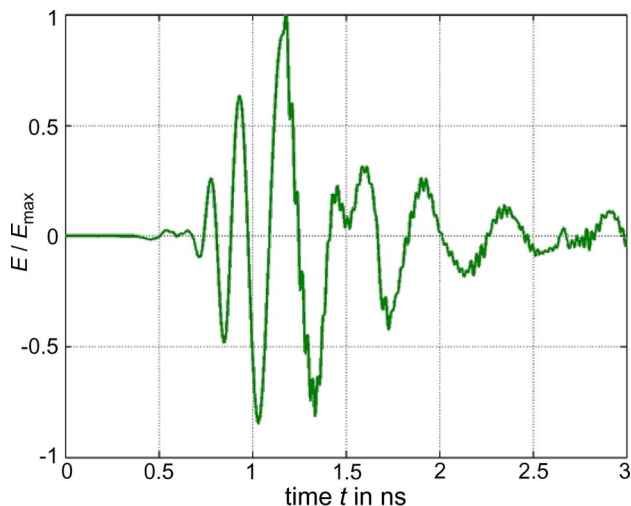


Fig. 18. Simulated impulse response of the Log-Per antenna (Fig. 16) in the main beam direction.

where the characteristics are determined to $\tau_{FWHM} = 805$ ps and $\tau_{r=0.22} = 605$ ps.

In Fig. 19, the gain $H(f, \theta)$ of the Log-Per antenna is shown. The antenna exhibits a relatively constant and stable radiation pattern over the frequency range. The collapse of the transfer function in main beam direction at particular frequencies and simultaneous side radiation at the same frequencies can be noticed. This is due to the excitation of higher order modes, e.g., λ -resonances, of the “ $\lambda/2$ -dipoles.”

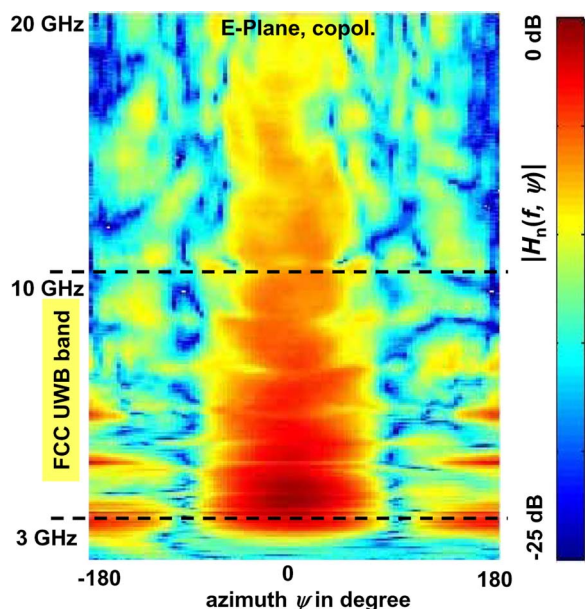


Fig. 19. Measured transfer function $|H(f, \theta)|$ of the Log-Per antenna versus frequency in the E-plane.

Table 2 UWB Parameters of the Log-Per Antenna of Fig. 17 in Main Beam Direction

Parameter	Value
p_{max} in m/ns	0.13
τ_{FWHM} in ps	805
\bar{G} in dBi	4.5
G_{max} in dBi	6.8
$\tau_{r=0.22}$ in ps	605

The main parameters of the Log-Per antenna of Fig. 16 are shown in Table 2.

E. Electrically Small Antennas

Electrically small antennas [25] are for any desired UWB operation “equally bad” concerning impedance matching and radiation. These antennas are far below resonance

$$a < \lambda_0/5 \tag{17}$$

which is specifying the antenna dimensions, a being the size of the radiating element (not the ground plane). Thus similar conditions for all frequencies exist. With a proper impedance transformation, the antennas can be made UWB. Typical candidates are the different types of D-dot probe antennas, small monopole antennas [26], and the Hertzian dipole.

In Fig. 20, a typical rotational symmetric UWB monocone antenna with a height of 20 mm ($\lambda/5$ at 3 GHz) is shown. The monocone antenna, as an asymmetric structure, does not require any balun for an asymmetric feed line; however, it needs (in theory) an infinite ground plane, which is cut for practical applications. For the regarded bandwidth, monocone antennas with a ground plane diameter larger than 40 mm (see Fig. 22) exhibit a return loss below $S_{11} < -10$ dB. For smaller ground planes, the matching becomes difficult for a 50Ω reference impedance. The finite ground plane also affects the stability of the radiation pattern versus frequency and the impulse radiating properties. Just recently, an antenna has been proposed that overcomes this problem by



Fig. 20. Monocone antenna with enlarged ground plane, with $d = 80$ mm diameter.

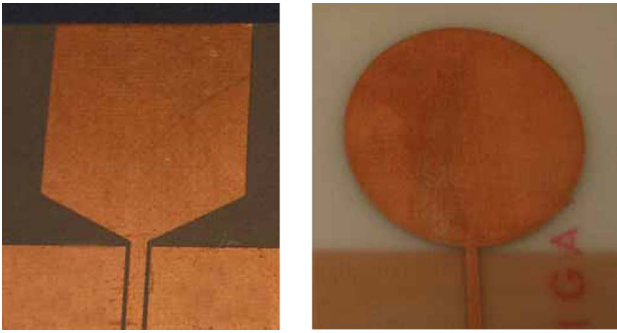


Fig. 21. Planar monopole antennas. (Left) CPW fed; (right) microstrip line fed with ground plane on the bottom side [28], [29].

compensating the dominating antenna capacity of electrically small antennas by inductive coupling to sectorial loops [27].

The monocone properties can be well approximated by the planar structures like planar monopoles (Fig. 21). These are very well suited for short-range communications, as they can easily be integrated with different planar lines and circuits.

The monocone antenna has an omnidirectional radiation pattern in H -plane. The impulse response $h(t)$ and gain $G(f)$ for a monocone antenna with reduced ground plane ($d = 40$ mm) are shown in the E -plane in Figs. 22 and 23, respectively. It can be seen that the impulse response is short, which indicates small ringing, and the antenna radiates over a wide elevation angle θ from $10^\circ < \theta < 90^\circ$ with a relatively constant gain $G(f)$. At higher frequencies the radiation is more upwards and a second beam emerges from the ground plane. Because of

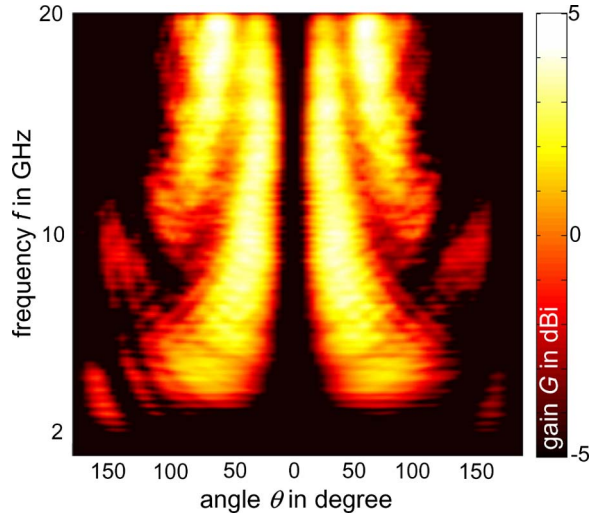


Fig. 23. Measured gain $G(f, \theta)$ of monocone antenna versus frequency in the E -plane.

the omnidirectional character of the antenna, the small $\tau_{FWHM} = 75$ ps value of the antenna impulse response, and the nearly frequency-independent gain, the monocone antenna is often applied for channel measurements.

In narrow-band operations, it is assumed that the antenna radiates identical signals in all directions of the antenna characteristic $C(\theta, \psi)$. In ultra-wide-band, this cannot be taken for granted, as will be shown for the monocone antenna. Fig. 24 shows the impulse response of the monocone antenna for $\psi = \text{const.}$ versus the elevation angle θ . It can clearly be seen that the radiated signals are elevation angle θ dependent.

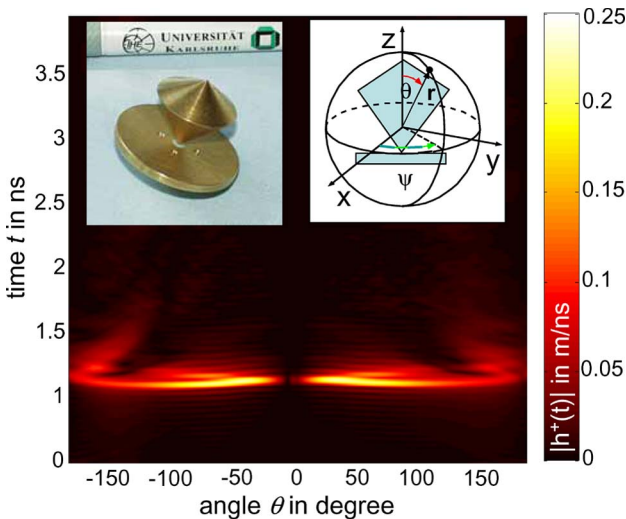


Fig. 22. Monocone antenna and its measured impulse response $|h^+(t)|$ in the E -plane (ground plane diameter $d = 40$ mm).

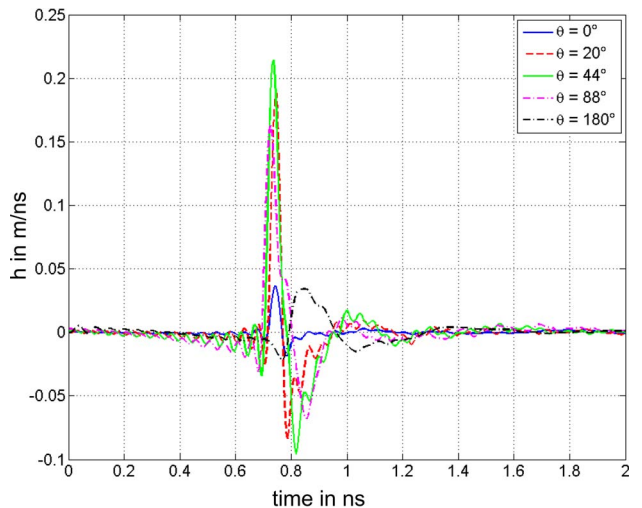


Fig. 24. Measured impulse response $h(t, \theta, \psi = 90^\circ)$ as a function of elevation θ for the monocone antenna.

In a multipath environment, these signals overlap at the receiver, which may cause severe distortion. Proper channel models can be used to study these effects [30].

IV. UWB ANTENNA SYSTEM ASPECTS

In practice from a system point of view, two cases for UWB have to be distinguished:

- multiple narrow bands, e.g., OFDM (ECMA-368 Standard);
- pulsed operation (IEEE 802.15.4a).

The first case can usually be treated like the well-known narrow-band operations. The relevant criteria are well covered by the frequency-dependent transfer function $\mathbf{H}(f, \theta, \psi)$. Antennas for these applications can be all earlier discussed types, especially also the Log-Per antenna.

The second case needs a closer look. If in a pulsed operation for radar or communications the full FCC bandwidth from 3.1 to 10.6 GHz, i.e., 7.5 GHz, is covered—for example, with the derivative of the Gaussian pulse with $\tau_{\text{FWHM}} = 88$ ps—then the transient behavior, the impulse response $\mathbf{h}(t, \theta, \psi)$ of the antenna, has to be taken into account. In this case, the impulse distortion in the time domain and in the spatial domain have to be examined for compatibility. An adverse behavior of the impulse response $\mathbf{h}(t, \theta, \psi)$, with the following problems:

- low peak magnitude $p(\theta, \psi)$;
- very wide pulse width τ_{FWHM} ;
- long ringing τ_r

has influence on the system characteristics, for example, on:

- the received signal strength $u_{\text{Rx}}(t)$, (S/N);
- the data rate in communications;
- the resolution in radar.

These adverse effects set requirements for the antennas but also for the other UWB hardware front-end elements like amplifiers, filters, equalizers, detectors, and so on. These requirements restrict the potential antennas to small antennas or traveling wave antennas. Candidates are:

- monocone antenna;
- bowtie antenna;

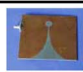
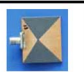
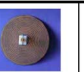
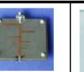

					
Peak value p in m/ns	0.35	0.13	0.10	0.13	0.23
τ_{FWHM} in ps	135	140	290	805	75
$\tau_{r=0.22}$ in ps	150	185	850	605	130

Fig. 25. Comparison of characteristic parameters of the presented UWB antennas.

- Vivaldi antenna;
- horn antenna.

All antennas with resonances or spurious surface currents are bad candidates and should be disregarded for time-domain operation. Among them is definitely the Log-Per antenna.

For certain cases where circular polarization is required, further restrictions hold. A logarithmic spiral antenna, e.g., can only radiate circular polarization if the pulse duration is longer than the equivalent circumference of the active radiating zone. For 88 ps pulses, this equivalent circumference should be less than 2.6 cm, which may contradict the radiation requirement.

These statements make clear that for UWB in extension to research at the component level, also research on the system level has to be performed.

V. CONCLUSION

Ultra-wide-band as an emerging technology requires for the antenna characterization a thorough knowledge of the behavior in time domain, in frequency domain, and, in certain cases, in the spatial domain. It has been shown that for ultra-wide-band, certain antenna classes can be defined according to their radiating characteristics. In Fig. 25, typical, relevant data of the discussed UWB antennas are compared. ■

REFERENCES

- [1] A. Shlivinski, E. Heyman, and R. Kastner, "Antenna characterization in the time domain," *IEEE Trans. Antennas Propag.*, vol. 45, pp. 1140–1149, Jul. 1997.
- [2] A. A. Smith, "Received voltage versus antenna height," *IEEE Trans. Electromagn. Compat.*, vol. EMC-11, pp. 104–111, Aug. 1969.
- [3] W. Sörgel, S. Schulteis, S. Knörzer, and W. Wiesbeck, "Deconvolution of the antennas from directional UWB channel measurements," in *Proc. Joint 9th Int. Conf. Electromagn. Adv. Applicat. (ICEAA)/ 11th Eur. Electromagn. Struct. Conf. (EESC)*, Torino, Italy, Sep. 2005, pp. 589–593.
- [4] W. Sörgel and W. Wiesbeck, "Influence of the antennas on the ultra wideband transmission," *EURASIP J. Appl. Signal Process. (Special Issue on UWB—State of the Art)*, pp. 296–305, Mar. 2005.
- [5] E. Farr and C. Baum, *Time domain characterization of antennas with TEM feeds*, Sensor and Simulation note 426, Oct. 1998.
- [6] FCC, *Revision of Part 15 of the commission's rules regarding ultra wideband transmission systems*, ET Docket 98-153, FCC 02-48, Feb. 14, 2002.
- [7] Commission of the European Communities, "Commission decision on allowing the use of the radio spectrum for equipment using ultra-wideband technology in a harmonised manner in the Community," *Official J. Eur. Union*, Feb. 21, 2007.
- [8] H. G. Schantz, "A brief history of UWB antennas," *IEEE Aerosp. Electron. Syst. Mag.*, vol. 19, pp. 22–26, Apr. 2004.
- [9] D.-H. Kwon, "Effect of antenna gain and group delay variations on pulse-preserving capabilities of ultrawideband antennas," *IEEE Trans. Antennas Propag.*, vol. 54, pp. 2208–2215, Aug. 2006.
- [10] R. P. Meys, "A summary of the transmitting and receiving properties of antennas," *IEEE Antennas Propag. Mag.*, vol. 42, pp. 49–53, Jun. 2000.
- [11] E. K. Miller and F. J. Deadrick, "Visualizing near-field energy flow and radiation," *IEEE Antennas Propag. Mag.*, vol. 42, pp. 46–54, Dec. 2000.
- [12] D. Schaubert, E. Kollberg, T. Korzeniowski, T. Thungren, J. Johansson, and K. Yngvesson, "Endfire tapered slot antennas on dielectric substrates," *IEEE Trans. Antennas Propag.*, vol. AP-33, pp. 1392–1400, Dec. 1985.
- [13] V. H. Rumsey, *Frequency-Independent Antennas*. New York: Academic, 1966.
- [14] P. E. Mayes, "Frequency-independent antennas and broad-band derivatives thereof," *Proc. IEEE*, vol. 80, pp. 103–112, Jan. 1992.

- [15] C. A. Balanis, *Antenna Theory: Analysis and Design*, 2nd ed. New York: Wiley, 1997, pp. 542–544.
- [16] E. Gschwendtner and W. Wiesbeck, “Ultra-broadband car antennas for communications and navigation applications,” *IEEE Trans. Antennas Propag.*, vol. 51, pp. 2020–2027, Aug. 2003.
- [17] Y. Mushiake, “Self-complementary antennas,” *IEEE Antennas Propag. Mag.*, vol. 34, pp. 23–29, Dec. 1992.
- [18] H. G. Booker, “Slot aerials and their relation to complementary wire aerials (Babinet’s principle),” *J. Inst. Elect. Eng.*, pp. 620–627, 1946.
- [19] B. H. Burdine, “The spiral antenna,” Massachusetts Inst. of Technol., Research Lab. Tech. Rep., Apr. 1955.
- [20] G. Deschamps, “Impedance properties of complementary multiterminal planar structures,” *IEEE Trans. Antennas Propag.*, vol. AP-7, pp. 371–378, Dec. 1959.
- [21] J. Dyson, “The equiangular spiral antenna,” *IEEE Trans. Antennas Propag.*, vol. AP-7, pp. 181–187, Apr. 1959.
- [22] D. H. Werner, R. L. Haupt, and P. L. Werner, “Fractal antenna engineering: The theory and design of fractal antenna arrays,” *IEEE Antennas Propag. Mag.*, vol. 41, pp. 37–58, Oct. 1999.
- [23] R. Pantoja, A. Sapienza, and F. M. Filho, “A microwave printed planar log-periodic dipole array antenna,” *IEEE Trans. Antennas Propag.*, vol. AP-35, pp. 1176–1178, Oct. 1987.
- [24] C. Peixeiro, “Design of log-periodic dipole antennas,” *Proc. Inst. Elect. Eng. Microw., Antennas Propag.*, vol. 135, no. 2, pt. H, pp. 98–102, Apr. 1988.
- [25] T. Yang, S.-Y. Suh, R. Nealy, W. A. Davis, and W. L. Stutzman, “Compact antennas for UWB applications,” *IEEE Aerosp. Electron. Syst. Mag.*, vol. 19, pp. 16–20, May 2004.
- [26] C. Harrison, Jr. and C. Williams, Jr., “Transients in wide-angle conical antennas,” *IEEE Trans. Antennas Propag.*, vol. AP-13, pp. 236–246, Mar. 1965.
- [27] N. Behdad and K. Sarabandi, “A compact antenna for ultrawide-band applications,” *IEEE Trans. Antennas Propag.*, vol. 53, pp. 2185–2192, Jul. 2005.
- [28] C.-C. Lin, Y.-C. Kan, L.-C. Kuo, and H.-R. Chuang, “A planar triangular monopole antenna for UWB communication,” *IEEE Microw. Compon. Lett.*, vol. 15, pp. 624–626, Oct. 2005.
- [29] X. Chen, J. Liang, P. Li, L. Guo, C. C. Chiau, and C. G. Parini, “Planar UWB monopole antennas,” in *Proc. Microw. Conf. (APMC 2005)*, Dec. 4–7, 2005, vol. 1.
- [30] A. F. Molisch, J. R. Foerster, and M. Pendergrass, “Channel models for ultrawide-band personal area networks,” *IEEE Wireless Commun.*, vol. 10, pp. 14–21, Dec. 2003.

ABOUT THE AUTHORS

Werner Wiesbeck (Fellow, IEEE) received the Dipl.-Ing. (M.S.E.E.) and Dr.-Ing. (Ph.D.E.E.) degrees from the Technical University Munich, Germany, in 1969 and 1972, respectively.

From 1972 to 1983, he was with AEG-Telefunken in various positions, including that of Head of R&D of the Microwave Division in Flensburg and Marketing Director Receiver and Direction Finder Division, Ulm. During this period, he had product responsibility for millimeter-wave radars, receivers, direction finders, and electronic warfare systems. From 1983 to 2007, he was Director of the Institut für Hochfrequenztechnik und Elektronik, University of Karlsruhe (TH), where he had been Dean of the Faculty of Electrical Engineering and is now Distinguished Scientist with the Karlsruhe Institute of Technology. Research topics include electromagnetics, antennas, wave propagation, communications, radar, and remote sensing. In 1989 and 1994, respectively, he spent a six-month sabbatical with the Jet Propulsion Laboratory, Pasadena, CA. He is a member of an Advisory Committee of the EU-Joint Research Centre (Ispra/Italy). He is an advisor to the German Research Council (DFG), to the Federal German Ministry for Research (BMBF), and to industry in Germany.

Dr. Wiesbeck is an Honorary Life Member of IEEE GRS-S, a member of the Heidelberger Academy of Sciences, and a member of acatech (German Academy of Engineering and Technology). He is a member of the IEEE GRS-S AdCom (1992–2000), Chairman of the GRS-S Awards Committee (1994–1998, 2002–), Executive Vice President IEEE GRS-S (1998–1999), President of IEEE GRS-S (2000–2001), Associate Editor IEEE-AP Transactions (1996–1999), and past Treasurer of the IEEE German Section (1987–1996, 2003–2007). He has been General Chairman of the 1988 Heinrich Hertz Centennial Symposium, the 1993 Conference on Microwaves and Optics (MIOP '93), the Technical Chairman of International mm-Wave and Infrared Conference 2004, Chairman of the German Microwave Conference GeMIC 2006, and a member of the scientific committees and Technical Program Committees of many conferences. He has received many awards, most recently the IEEE Millennium Award, the IEEE GRS Distinguished Achievement Award, the Honorary Doctorate (Dr. h.c.) from the University Budapest/Hungary, the Honorary Doctorate (Dr.-Ing. E.h.) from the University Duisburg/Germany, and the IEEE Electromagnetics Award 2008.



Grzegorz Adamiuk (Student Member, IEEE) received the Dipl.-Ing. degree in electrical engineering from Technical University of Gdansk, Poland, and the Universität Karlsruhe (TH), Germany, in 2006. He is currently pursuing the Ph.D.E.E. degree at the Universität Karlsruhe.

Since 2006, he has been with the Institut für Hochfrequenztechnik und Elektronik, Universität Karlsruhe, as a Research Associate. His main research topic is UWB technology with focus on UWB antennas and channel characterization.



Christian Sturm (Student Member, IEEE) received the Dipl.-Ing. degree in electrical engineering and information technologies from Universität Karlsruhe (TH), Germany, in 2005.

Since February 2005, he has been with the Institut für Hochfrequenztechnik und Elektronik, Universität Karlsruhe, as a Research Associate. His main research areas are multiple antenna transmission systems and the propagation of ultrawide-band signals in indoor scenarios. He has experience in signal processing and antenna array processing techniques. He is a Lecturer for the Carl-Cranz-Series for Scientific Education and for the European School of Antennas.

